Boletim da Sociedade Astronômica Brasileira, **35**, no. 1, 250-254

Analysis of the spiral structures of the grand design galaxies IC 4566 and NGC 768 using Fourier Transforms

S. F. Costa[1], I. Rodrigues[1] & L. A. Caritá[2]

[1] Universidade do Vale do Paraíba, 2911 Shishima Hifumi Avenue, São José dos Campos, SP, 12244-390, Brazil
e-mail: steefaria@gmail.com
e-mail: irapuan.rodrigues@gmail.com
[2] Instituto Federal de Educação, Ciência e Tecnologia de São Paulo, Rod. Pres. Dutra, São José dos Campos, SP, 12223-201, Brazil
e-mail: prof.carita@ifsp.edu.br

Abstract. The objective of this work is to apply Fourier Transforms for the analysis of structures in two grand design spiral galaxies: IC 4566 and NGC 768. For this purpose, images from the DESI Legacy Imaging Survey in the g, r, and z bands were used, and programs in PYTHON were developed for method implementation. Initially, we applied two-dimensional Fourier Transform to determine the dominant components (m) in each of the spiral structures, along with the measurement of the pitch angle α for each mode. Subsequently, one-dimensional Fourier Transform was implemented to determine corotation resonance and the character of the spiral pattern in each galaxy. As a result, IC 4566 and NGC 768 exhibited a dominant mode of $m = 2$ with $|\alpha| \approx 16.9$ and $|\alpha| \approx 18.9$, respectively. The methods provide a good characterization of grand design spiral galaxy structures, and the obtained pitch angle values closely align with those reported in other studies and techniques.

Resumo. O objetivo deste trabalho é aplicar as Transformadas de Fourier para análise das estruturas presentes em duas galáxias espirais *grand design*: IC 4566 e NGC 768. Para isso, foram utilizadas imagens do DESI Legacy Imaging Survey nas bandas g, r e z e criados programas em PYTHON para implementação dos métodos. Primeiramente, aplicamos a Transformada de Fourier bidimensional para determinação das componentes (m) dominantes em cada uma das estruturas espirais, além da medição do *pitch angle* α de cada modo. Em seguida, foi implementada a Transformada de Fourier unidimensional para determinação da ressonância de corrotação e do caráter do padrão espiral de cada galáxia. Como resultado, as galáxias IC 4566 e NGC 768 apresentaram como modo dominante $m = 2$ com $|\alpha| \approx 16.9$ e $|\alpha| \approx 18.9$, respectivamente. Os métodos apresentam boa caracterização das estruturas espirais de galáxias *grand design* e os valores obtidos para o *pitch angle* aproximam-se de valores apresentados em outros estudos e técnicas.

Keywords. Galaxies: spiral – Galaxies: structure – Techniques: image processing

1. Introduction

The spiral structure is the most distinctive feature of disk galaxies, and although they have been studied for over a century, their nature is still debated. Several researchers have worked to develop an objective method for the analysis and classification of spiral galaxies. The Fourier Transform method applied to images of spiral galaxies was initially proposed by Kalnajs (1975), first used with the aim of retrieving information about the distributions of HII regions. Authors such as Considère & Athanassoula (1992); Iye et al. (1982); Considère & Athanassoula (1988); Puerari & Dottori (1990, 1992); Vera-Villamizar et al. (2001) have extensively employed this method. In Puerari & Dottori (1997) , a method was developed to analyze the azimuthal gradient of ages through spiral arms using one-dimensional Fourier Transform, enabling the determination of the corotation radius for galaxies NGC 1832 and NGC 7479. Furthermore, one-dimensional and two-dimensional Fourier techniques are widely adopted for measuring the pitch angle of spiral arms (Savchenko & Reshetnikov 2013; Yu et al. 2018; Yu & Ho 2018).

2. Methodologies

2.1. Spiral structure

In polar coordinates, a logarithmic spiral can be defined as:

$$r = r_0 e^{-\frac{m}{p}\theta}, \tag{1}$$

where m is the number of arms, r and θ are polar coordinates, and p is the variable related to the spiral's pitch angle α through the expression:

$$\tan(\alpha) = -\frac{m}{p} \qquad \Rightarrow \qquad \alpha = \arctan\left(-\frac{m}{p}\right). \tag{2}$$

The pitch angle, represented by α, measures the degree of winding of a galaxy's spiral arms.

2.1.1. Character of the spiral pattern

Another important factor is the determination of the leading or trailing character of the spiral arms. Analyzing the winding from the inside out, a spiral arm is of the leading type when it is wound in the same direction as the rotation of the galactic disk. When the winding direction of the spiral arm is opposite to the direction of the galactic disk's rotation, we have a trailing arm (Fig. 1).

2.1.2. Corotation resonance

Consider that the spiral pattern has an approximately constant angular velocity, while the gas and star disk exhibits differential rotation. We refer to the corotation radius as the radius at which the angular velocity of the pattern (Ω_p) equals the angular velocity of the disk (Ω), i.e., ($\Omega_p = \Omega$). Thus, in the region inside the

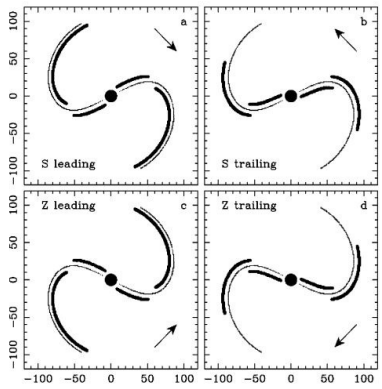

FIGURE 1: Position of the shock front (heavy line) with respect to the wave front of the spiral density wave (DW, light line) for S-type spirals: (a) leading and (b) trailing; Z-type spirals: (c) leading and (d) trailing. In each panel, the arrows indicate the direction of the disk's rotation. The displacement of the shock front at the corotation radius is noticeable. (Figure extracted from Puerari & Dottori 1997).

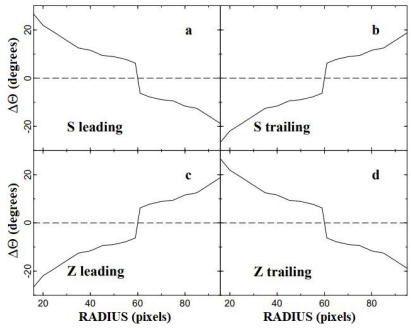

FIGURE 2: Relative behavior of the phase $\Theta(r)$ of the DW (dashed line) and the shock front (solid line) for the cases presented in Fig. 1. (Adapted from Villamizar (2001)).

corotation radius, the rotation speed of the disk is greater than that of the pattern ($\Omega_p < \Omega$), while for outer radii, the opposite occurs ($\Omega_p > \Omega$). Consequently, the scenario of star formation is described as follows: within the corotation radius, gas and stars from the disk are 'colliding' with the pattern, while outside the corotation radius, the pattern 'collides' with the disk material. This collision creates the shock front in the spiral arms, and as a result, a displacement of the shock front is observed from the concave side to the convex side of the spiral arm at the corotation radius (Fig. 1). Therefore, we observe an inversion of the azimuthal gradient of stellar ages at the corotation radius, due to the shock front being associated with star formation.

2.2. Analysis methods

We will use the one-dimensional Fourier Transform method to determine the corotation radius and the two-dimensional Fourier Transform method for the morphological study of the spiral structure, identifying the components of the pattern and their significance, as well as the pitch angle for each mode.

2.2.1. One-dimensional Fourier Transform

Let $f : \mathbb{R} \to \mathbb{C}$ be a function that satisfies the conditions of integrability. We define the Fourier Transform of $f(x)$ as:

$$\mathcal{F}[f(x)] = F(k) = \int_{-\infty}^{+\infty} f(x) e^{-ikx}\, dx. \tag{3}$$

In Puerari & Dottori (1997), the point of phase reversal for the relative phases of the density wave (hereafter, DW) (Θ_{dw}) and the shock front (Θ_{sf}) was detected through the Fourier Transform applied to azimuthal profiles $I_r(\theta)$, based on the scenario described by Roberts (1969). This point of reversal indicates the corotation radius. In this context, we can express the one-dimensional Fourier Transform as:

$$\mathcal{F}_m(r) = \int_{-\infty}^{+\infty} I_r(\theta) e^{-im\theta} d\theta, \tag{4}$$

where m is the number of arms. In practice, the integrals are calculated from a minimum radius to a maximum radius.

The phase Θ is obtained through the expression:

$$\Theta(r) = \arctan \frac{\Im[\mathcal{F}_m(r)]}{\Re[\mathcal{F}_m(r)]}, \tag{5}$$

where $\Re$ and $\Im$ correspond to the real and imaginary parts of the complex Fourier coefficients, respectively.

To detect the point of phase reversal of the relative phases between the DW and the shock front (Fig. 1) from images of a galaxy, we need two images of the galaxy in different bands: one bluer band that shows recent stellar population (shock front) and another redder band that shows older stars (DW). Using Eqs. (4) and (5), we calculate the phase Θ for each image, namely Θ_{sf} and Θ_{dw}. Next, the phase difference in the two filters is calculated, i.e., $\Delta\Theta = \Theta_{sf}$ - Θ_{dw}, and the phase difference diagram is plotted. This diagram also allows the identification of the leading or trailing character of the spiral structure when the type of spiral arms (S or Z) is known, as presented in Fig. 2. The intersection point between these two lines indicates the corotation radius.

2.2.2. Two-dimensional Fourier Transform

Similarly, for a function $f : \mathbb{R} \times \mathbb{R} \to \mathbb{C}$, we will have:

$$\mathcal{F}[f(x,y)] = F(k,l) = \int_{-\infty}^{+\infty} \int_{-\infty}^{+\infty} f(x,y) e^{-i(kx+ly)}\, dxdy \tag{6}$$

and

$$\mathcal{F}^{-1}[F(k,l)] = f(x,y) = \frac{1}{4\pi^2} \int_{-\infty}^{+\infty} \int_{-\infty}^{+\infty} F(k,l) e^{i(kx+ly)}\, dkdl, \tag{7}$$

where Eq. (6) represents the two-dimensional Fourier Transform, and Eq. (7) represents the two-dimensional Inverse Fourier Transform.

The continuous density distribution $I(u,\theta)$, corresponding to the discrete matrix $I(u_k,\theta_l)$, can be expanded into a Fourier series in the azimuthal angle θ and an integral over the logarithm of the radius u. Therefore, we have:

$$I(u,\theta) = \frac{1}{2\pi} \sum_{m=0}^{+\infty} \int_{-\infty}^{+\infty} A(p,m) e^{i(pu+m\theta)}\, dp \tag{8}$$

where m is the azimuthal wave number or the number of spiral arms, and p is the logarithmic radial wave number or a measure of the direction and degree of winding of the spiral arms. The Fourier coefficient, $A(p,m)$, represents the intensity of the component that has a logarithmic spiral shape with m arms and a pitch angle $\alpha = \arctan\left(-\frac{m}{p}\right)$.

Table 1: Propriedades das galáxias selecionadas.

Galaxy	Type	PA(deg)	e	m	$\lvert\alpha\rvert$
IC 4566	Sb	153	0.31	2	$16.2° \pm 1.2$
NGC 768	Sc	25	0.53	2	$17.5° \pm 1.3$

Note. Column 1: galaxy name. Column 2: morphological type of the galaxy according to the Hubble classification. Column 3: position angle. Column 4: ellipticity. Column 5: mode used to calculate the pitch angle. Column 6: pitch angle of the spiral arm. The data in the table were sourced from Yu & Ho (2019).

We can obtain the Fourier coefficient $A(p,m)$ by performing the Fourier transform on $I(u,\theta)$, such that:

$$A(p,m) = \frac{1}{\sum_{k'=1}^{m'}\sum_{l'=1}^{n'} w_{k'l'}} \sum_{k'=1}^{m'}\sum_{l'=1}^{n'} w_{k'l'} e^{-i(pu+m\theta)}, \quad (9)$$

where w_{kl} is the weight of the point (k,l) located at coordinates (r_{kl},θ_{kl}) and $u_{kl} = \ln(r_{kl})$. Similar to the one-dimensional Fourier Transform, the integrals are calculated from a minimum radius to a maximum radius. To obtain the matrix $A(p_i,m)$, the Fast Fourier Transform (FFT) algorithm was used[1]. We employed a basis with 6 logarithmic spirals, with the azimuthal wave number (or number of arms) in the range $0 \leq m \leq 6$ and the logarithmic radial wave number in the range $-50 \leq p \leq 50$ with $\Delta m = 1$ and $\Delta p = 0.25$. With m being the number of arms, we refer to each m as a component or mode. In this context, the galaxy will be a sum of m components, one of which will be the dominant component—meaning, the component in which the peak amplitude is the highest in the Fourier spectrum. This nomenclature is commonly used in the field.

We can reconstruct the image of the galaxy by performing the inverse transform of the complex functions $A(p,m)$. Thus, the surface density (complex function) is calculated through the equation:

$$S(u,\theta) = \sum_m S_m(u) e^{im\theta} \quad (10)$$

where

$$S_m(u) = \frac{\sum_{k'=1}^{m'}\sum_{l'=1}^{n'} w_{k'l'}}{e^{2u}4\pi^2} \int_{-\infty}^{+\infty} G_m(p) A(p,m) e^{ipu} dp \quad (11)$$

and

$$G_m(p) = e^{-\frac{1}{2}\left[\left(\frac{p-p_{max}}{5}\right)^2\right]} \quad (12)$$

where p_{max} is the value of p at which the spectrum has the maximum amplitude for a given m.

2.3. Images

We selected two spiral galaxies for analysis: IC 4566 and NGC 768, using images in the g (green), r (red), and z (near-infrared) bands taken from the DESI Legacy Survey. These images cover 138.2×138.2 $arcsec^2$, with a scale of 0.27 $arcsec\ pixel^{-2}$. Table 1 contains compiled data from Yu & Ho (2019).

[1] This routine is part of a series of algorithms presented in the book *Numerical Recipes in C* (Press et al. 1992).

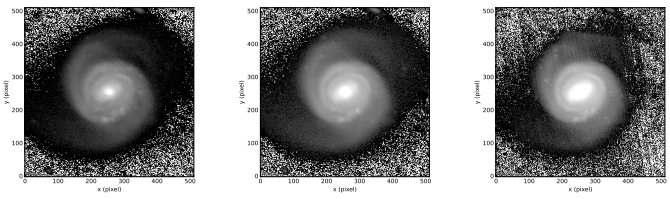

(a) (b) (c)

FIGURE 3: Images used for the galaxy IC 4566 without field stars and deprojected in the g, r, and z filters, respectively.

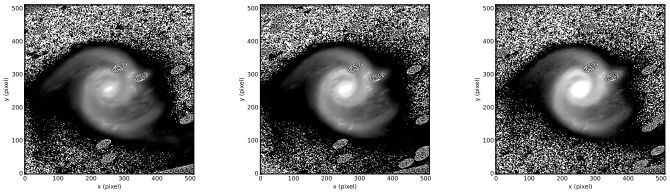

(a) (b) (c)

FIGURE 4: Images used for the galaxy NGC 768 without field stars and deprojected in the g, r, and z filters, respectively.

2.4. Image Preprocessing

2.4.1. Star Subtraction

The field stars present in the galaxy images are responsible for generating spurious frequencies in the Fourier Transform. Therefore, prior to the analysis, an edit was performed on the images to remove the field stars. This image processing step was carried out using the *IRAF* software with the *imedit* routine.

2.4.2. Deprojection

For the analysis of spiral structures, it is necessary for galaxies to be in a 'face-on' orientation. Therefore, the images were deprojected before applying our analysis methods (Figs. 3 and 4).

For the completion of this study, programs were created in PYTHON to carry out all tasks. For image deprojection, the values of PA and ellipticity, as per Tab. 1, were employed.

3. Results

3.1. IC 4566

The two-dimensional Fourier Transforms in IC 4566 for the g, r, and z bands were calculated in a radius range from 9.0 kpc to 25.5 kpc. The Fourier spectra, shown in Fig. 5, indicate that the component $m = 2$ is dominant in the images g, r, and z, with the other components contributing less. The values obtained in each band are similar, showing minimal variations. In Tab. 2 the values of the highest peaks in the Fourier spectrum are presented. By calculating the average of the obtained values for the pitch angle in the g, r, and z bands at $m = 2$ (dominant component), we have $|\alpha| \approx 16.9°$, consistent with the value obtained in Yu & Ho (2019), as shown in Tab. 1.

Figure 6 contains the images of the Inverse Fourier Transforms of IC 4566 in the g, r, and z bands, calculated with the sum of components $m = 1,2,3,4,5$, and 6. In all three images, the symmetry and extension of the two spiral arms can be observed.

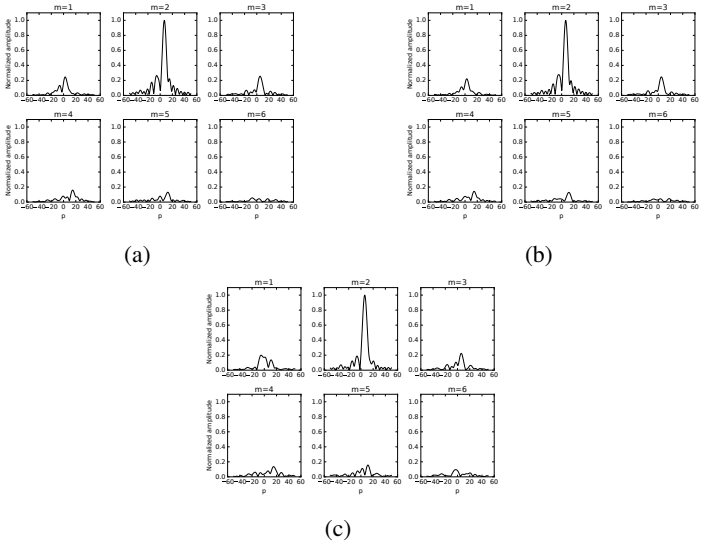

(a) (b)

(c)

FIGURE 5: Fourier coefficients $A(p,m)$ in the g, r, and z images of the galaxy IC 4566.

Table 2: Some values obtained in the Fourier spectrum for IC 4566.

Band	m	p	Amplitude	α
	2	6.75	1.00	-16.50
g	4	14.75	0.16	-15.17
	2	6.75	1.00	-16.50
r	4	14.75	0.14	-15.17
	2	6.25	1.00	-17.74
z	4	15.25	0.14	-14.70

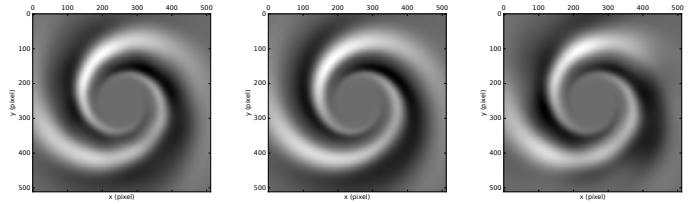

(a) (b) (c)

FIGURE 6: Images of the Inverse Transforms of IC 4566 for components $m = 1,2,3,4,5$, and 6 in the g, r, and z bands, respectively. Note that the recovered spiral is highlighted in white in the images.

With the aim of determining the corotation resonance in IC 4566, the one-dimensional Fourier Transform was applied to the g and z bands in a radius range from 2.0 kpc to 25.5 kpc (analyzing from the central part of the galaxy). Subsequently, the phase was calculated for each image, and the phase difference diagram was constructed (Fig. 7). This diagram indicates two corotation radii, approximately at 7.8 kpc and 16 kpc.

In the face of this scenario with two cutoff points, we will proceed as in Villamizar (2001) and apply the method to the images of the Inverse Fourier Transforms for $m = 2$ in order to determine the corotation radius and the character of the pattern accurately. Figure 8 shows the obtained phase difference diagram.

Comparing the results obtained in both cases, as there is an indication of a bar in this galaxy, we conclude that the corotation radius of IC 4566 is located at approximately 7.8 kpc, and the pattern's character is trailing. Regarding the cutoff identified at approximately 16 kpc with a leading pattern, it can be explained as a consequence of interactions with nearby galaxies, particularly IC 4566. This interaction influences the outer region of the spiral structure, giving rise to the emergence of a second corotation radius in the galaxy.

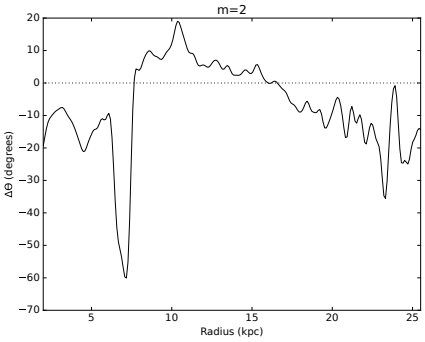

FIGURE 7: Phase difference diagram of the galaxy IC 4566 for $m = 2$ obtained from the phases in the g and z filters.

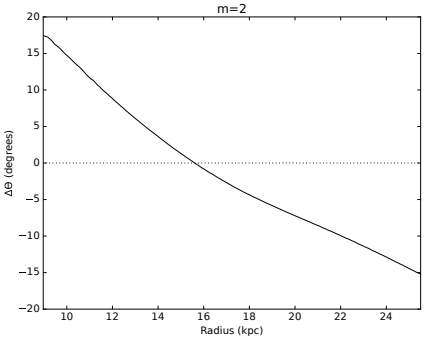

FIGURE 8: Phase difference diagram of the galaxy IC 4566 for $m = 2$ obtained from Inverse Transforms in the g and z filters.

Table 3: Some values obtained in the Fourier spectrum for NGC 768.

Band	m	p	Amplitude	α
g	2	-5.75	1.00	19.18
	4	-10.75	0.32	20.41
r	2	-5.75	1.00	19.18
	4	-10.75	0.31	20.41
z	2	-6.0	1.00	18.43
	4	-11.0	0.30	19.98

3.2. NGC 768

The two-dimensional Fourier Transform in NGC 768 for the g, r, and z bands was calculated in a radius range from 5.6 kpc to 32.0 kpc. The Fourier spectra, shown in Fig. 9, indicate that the component $m = 2$ is dominant in all three bands, and the other components contribute little. Table 3 presents the values of the highest peaks in the Fourier spectrum. By calculating the average of the obtained values for the pitch angle in the g, r, and z bands at $m = 2$ (dominant component), we obtain $|\alpha| \approx 18.9°$, which is close to the value obtained in Yu & Ho (2019), as displayed in Tab. 1.

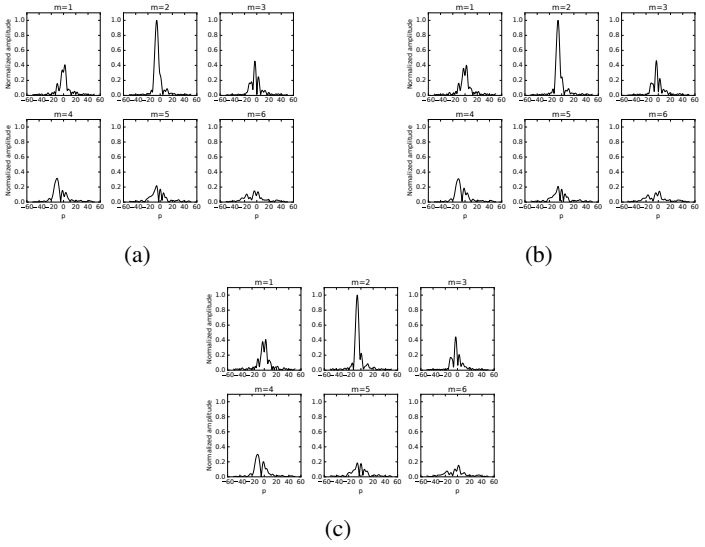

(a) (b)

(c)

FIGURE 9: Fourier coefficients $A(p,m)$ in the g, r, and z images of the galaxy NGC 768.

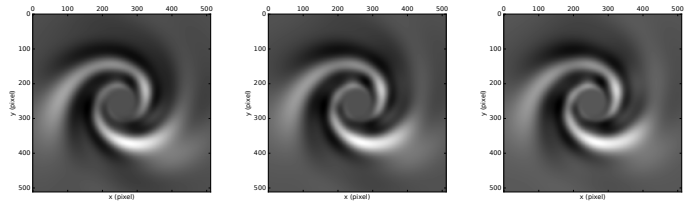

(a) (b) (c)

FIGURE 10: Images of the Inverse Transforms of NGC 768 for components $m = 1,2,3,4,5$, and 6 in the g, r, and z bands, respectively. Note that the recovered spiral is highlighted in white in the images.

Figure 10 contains the images of the Inverse Fourier Transforms of NGC 768 in the g, r, and z bands, calculated with the sum of components $m = 1,2,3,4,5$, and 6. We were able to recover the spiral structure well in all images, observing the symmetry and extension of the arms.

The one-dimensional Fourier Transform was applied to the g and z bands in a radius range from 2.5 kpc to 32.0 kpc. Figure 11 shows the obtained phase difference diagram. Due to noise, the cuts at radii smaller than 5 kpc and larger than 25 kpc can be discarded from the analysis.

Just like the previous galaxy, with these images, we have some possible corotation radii. Applying the method to the images of the Inverse Fourier Transforms for $m = 2$ and obtaining the phase difference diagram (Fig. 12), we can determine that the character of the pattern is trailing, and the corotation radius is at 15 kpc.

4. Conclusion

The Fourier Transforms are powerful methods for the analysis of structures in spiral galaxies, especially for grand design spiral galaxies. With the technique of two-dimensional Fourier Transform, we can determine the most relevant components in the spiral structure of galaxies, as well as obtain the pitch angle of the arms for each mode individually. Still using this technique, through the Inverse Transform, we can draw and recover the individual components or sum the main components of the spiral structure, allowing a good characterization of these structures for grand design galaxies. The analysis with the one-dimensional Fourier Transform enabled the determination of the corotation resonance of the galaxies, as well as the character of the spiral pattern. These two techniques complement each other for a morphological study of spiral galaxies, making the characterization of these structures more complete.

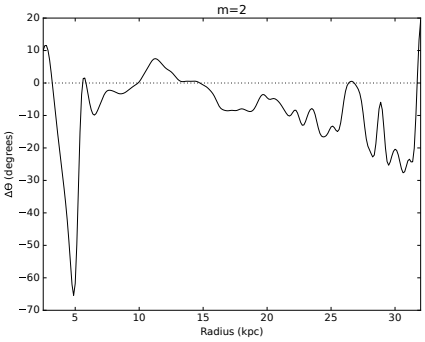

FIGURE 11: Phase difference diagram of the galaxy NGC 768 for $m = 2$ obtained from the phases in the g and z filters.

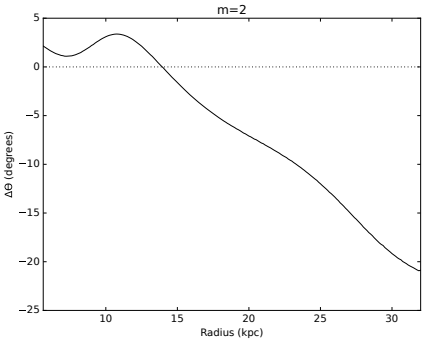

FIGURE 12: Phase difference diagram of the galaxy NGC 768 for $m = 2$ obtained from Inverse Transforms in the g and z filters.

Acknowledgements. This study was financed in part by the Coordenação de Aperfeiçoamento de Pessoal de Nível Superior – Brasil (CAPES) – Finance Code 001.

References

Considère S. & Athanassoula E. 1982, Astronomy and Astrophysics, 111, 28.
Considère S. & Athanassoula E. 1988, Astronomy and Astrophysics Supplement Series, 76, 365.
Iye, M. et al. 1982, The Astrophysical Journal, 256, 103.
Kalnajs A. J. 1975, La Dynamique des galaxies spirales, 241, 103.
Press, William H. et al,1992, Numerical Recipes in C: The Art of Scientific Computing, (Cambridge: Cambridge University Press), 59.
Puerari, I. & Dottori, H. 1990, Revista Mexicana de Astronomia y Astrofisica, 21, 126.
Puerari, I. & Dottori, H. 1992, Astronomy and Astrophysics Supplement Series, 93, 469.
Puerari, I. & Dottori, H. 1997, The Astrophysical Journal, 476, L73.
Roberts, W. 1969, The Astrophysical Journal, 158, 123.
Savchenko, S. S. & Reshetnikov, V. P. 2013, Monthly Notices of the Royal Astronomical Society, 436, 1074.
Vera-Villamizar, N. et al. 2001, The Astrophysical Journal, 547, 187.
Villamizar, N.V. 2001, Análise de Ressonâncias em Galáxias Espirais. Tese (Doutorado), Universidade Federal do Rio Grande do Sul.
Yu, S.-Y. et al. 2018, The Astrophysical Journal, IOP Publishing, 862, 13.
Yu, S.-Y. & Ho, L. C. 2018, The Astrophysical Journal, IOP Publishing, 869, 29.
Yu, S.-Y. & Ho, L. C, 2019, The Astrophysical Journal, 871, 194.